TD 91-2834

TNO Defence Research

AD-A256 545

TNO-report
PML 1991-54

Scaling laws for diffraction loading by air blast

June 1992
Copy no: - 2

Author(s):
Dr. E.A. Bakkum

TDCK RAPPORTENCENTRALE
Frederikkazerne, gebouw 140
v/d Burchlaan 31   **MPC 16A**
TEL. : 070-3166394/6395
FAX. : (31) 070-3166202
Postbus 90701
2509 LS Den Haag

DTIC
S ELECTE D
OCT 2 8 1992
A

Total Number of Pages:
(ex. distr. list and RDP)
30

Number of Annexes:
3

Number of Figures:
11

Number of Tables:
1

DO assignment no.:

Number of Copies:
17

Classification

Report:
UNCLASSIFIED

Title:
UNCLASSIFIED

Summary:
UNCLASSIFIED

Annex(es):
UNCLASSIFIED

92-28359

TNO 92 10 27 157

Summary

The assessment of the damage, which is done to structures by an explosion, depends both on the blast loading and the structural response. In the past scaling laws were developed for the description of simple blast loadings, thus eliminating the need for full-scale experiments. The aim of this work is to construct an approximate scaling law for complex blast loadings.

The blast loading on a model of a shelter was studied in the 40x40 cm^2 blast simulator of the TNO Prins Maurits Laboratory. The density distribution around the model was determined by means of flow visualization with a shearing interferometer. An approximate scaling law, which eliminates the dependency on the shock strength, is proposed for the time behaviour of the blast loading. The scaling law is confirmed by measurements of the density at various locations on the model, for shock strengths of 6.5 kPa and 33.2 kPa.

Samenvatting

De schatting van schade, die door een explosie wordt toegebracht aan constructies, is gebaseerd op de schokbelasting en op de eigenschappen van de constructie. In het verleden zijn schalingswetten afgeleid om eenvoudige schokbelastingen te beschrijven, waardoor de noodzaak voor onderzoek op ware grootte is vervallen. Het doel van deze studie is om een schalingswet af te leiden, die ingewikkelde schokbelastingen bij benadering beschrijft.

De schokbelasting op het model van een bunker werd bestudeerd in the 40x40 cm^2 schokbuis van het TNO Prins Maurits Laboratorium. De dichtheidsverdeling rond het model werd bepaald door stromingsvisualisatie met behulp van een differentiaal interferometer. Een schalingswet, die in goede benadering onafhankelijkheid is van de schoksterkte, wordt voorgesteld voor het tijdsgedrag van de schokbelasting. De schalingswet wordt bevestigd door metingen van de dichtheid op een aantal plaatsen op het model, bij schoksterktes van 6.5 kPa en 33.2 kPa.

CONTENTS

1   INTRODUCTION

When an explosion occurs, a blast wave is formed in the surrounding air. The sudden rise in pressure at the shock front of the blast wave can cause damage to structures in the neighbourhood of the explosion centre. The amount of damage is determined both by the blast loading and by the structural response due to the load.

In calculations of the blast load on structures it is common practice to obtain the strength and duration of the incident blast wave from scaling laws (Sachs scaling, [1]). The similarity principle states that it is sufficient to perform measurements for a single charge, say 1 kg of TNT, and then the behaviour of blast waves due to a charge with an arbitrary size can be derived from these results by means of scaling factors. The scaling factors remove the dimensional parameters in the governing equations and the physical situation is determined completely by a set of dimensionless so-called Pi terms. For instance, the peak pressure p_s of the shock caused by an explosion of a charge in free air is described by the equation $\Omega(p_s r^3/W, \rho_0 c_0^2 r^3/W) = 0$, where r is the distance from the centre, W is the charge size, and ρ_0 and c_0 are the density and sound velocity of ambient air.

The purpose of this work is to obtain scaling laws for the blast loading on structures, which include complicated wave phenomena like reflection and expansion processes. The study is part of the research programmes at the Prins Maurits Laboratory, which attempt to develop an integrated model for blast loading and structural response, and was funded by the TNO Division for National Defence Research. Chapter 2 discusses the application of the Buckingham Pi theorem and reviews an empirical model for the blast loading on a rectangular structure. A set of Pi terms is proposed for the description of blast loading during the diffraction phase. In Chapter 3 an experimental setup for the measurement of the blast loading on a structure in a shock tube is described. The results of the measurements and a discussion of the observed phenomena are contained in respectively Chapters 4 and 5. The conclusions of this study are given in Chapter 6.

2   A MODEL OF BLAST LOADING

2.1   Drag loading

It is common to consider two phases in the process of blast loading:
-   diffraction loading, which consists of the interaction of the shock front with the structure, and
-   drag loading, which is caused by the explosion-induced air flow.

This section discusses drag loading, where scaling techniques originating from the theory of fluid mechanics can be applied. In fluid mechanics scaling laws have been used with success for the description of steady fluid flows around obstacles. The physical process is determined completely by the velocity u_0 of the main stream, the fluid density ρ_0, the viscosity η and the dimension l of the obstacle. A possible choice for the dimensionless Pi term is the Reynolds number

$$R_e = \rho_0 \, u_0 \, l \, / \, \eta \tag{1}$$

A frictional force F will act on the surface of the obstacle and a dimensional analysis shows that it must take the form

$$F = C \frac{1}{2} \rho_0 \, u_0{}^2 \, l^2 \tag{2}$$

where C is a dimensionless quantity, called the drag coefficient. The value of the drag coefficient is determined by R_e and by the shape of the obstacle. For a laminar boundary layer and large values of R_e the drag coefficient becomes nearly independent of R_e [2]. The force F is called the drag force, the term

$$q_0 = \frac{1}{2} \rho_0 \, u_0{}^2 \tag{3}$$

is the dynamic pressure and $C \, q_0$ is called the drag pressure.

2.2   Diffraction loading on a rectangular structure

The loading of a structure by a blast wave during the diffraction phase varies with time and depends strongly on the profile of the blast wave. The basic problem in the construction of scaling laws for diffraction loading is that the occurring wave phenomena depend in a complicated way on the peak overpressure p_s of the shock (or equivalently, on its velocity U_s). Therefore, the scaling laws can only be approximations with a limited validity. In the present study the attention is focussed on the range of pressures p_s between 1 and 100 kPa, because it is the most interesting for the assessment of damage.

As an illustration, this section describes the blast loading on the front, the top and the back face of a rectangular structure with height H and length L. The shock front is plane and the overpressure p_s in the shock is constant, i.e. it is a uniform shock. The discussion presented below is valid for shocks with values of p_s up to 350 kPa [3]. The shock velocity is given by

$$U_s = c_0 \sqrt{1 + 6/7 \ (p_s/p_0)} \qquad (4)$$

where c_0 and p_0 are respectively the velocity of sound and the pressure of ambient air [3].

Figure 1a shows the reflection of the shock from the front face of the structure. The reflected over-pressure is given by

$$p_r = 2 \ p_s + 2.4 \ q \qquad (5)$$

where q is the dynamic pressure (see 2.1). The pressure gap between p_r and p_s is bridged by the formation of an expansion wave at the corner of the structure. According to Glasstone [3] the expansion wave causes a decay of the average pressure on the front face to the stagnation pressure

$$p_{stag} = p_s + C \ q \qquad (6)$$

in a time $t = 3 \ H/U_s$. The drag coefficient C is unity in this case.

In Figure 1b the shock front has passed the top and diffracts around the back edge. Glasstone assumes that the average pressure on the fully loaded top (i.e. for $t > L/U_s$) is given by equation (6) with $C = -0.4$ [3]. The expansion waves extend over the top face and vortices are formed at the edges, so the local pressure can deviate somewhat from the average pressure.

Finally, Figure 1c shows the reflection of the second expansion wave on the floor behind the struc-ture. According to Glasstone it requires an additional time $t = 4 \ H/U_s$ after the arrival of the shock at the back face for an average pressure to build up. The average pressure is given by equation (6) with $C = -0.3$ [3].

At this time the force on the structure is completely due to drag loading. Drag loading by blast waves with a long duration ('positive phase') can cause significant damage; however, for conven-tional explosives the wavelength of blast is usually comparable to the dimension of loaded structures and drag loading is of minor importance. In such cases damage is caused mainly by the large pres-sure differences in the phase of diffraction loading.
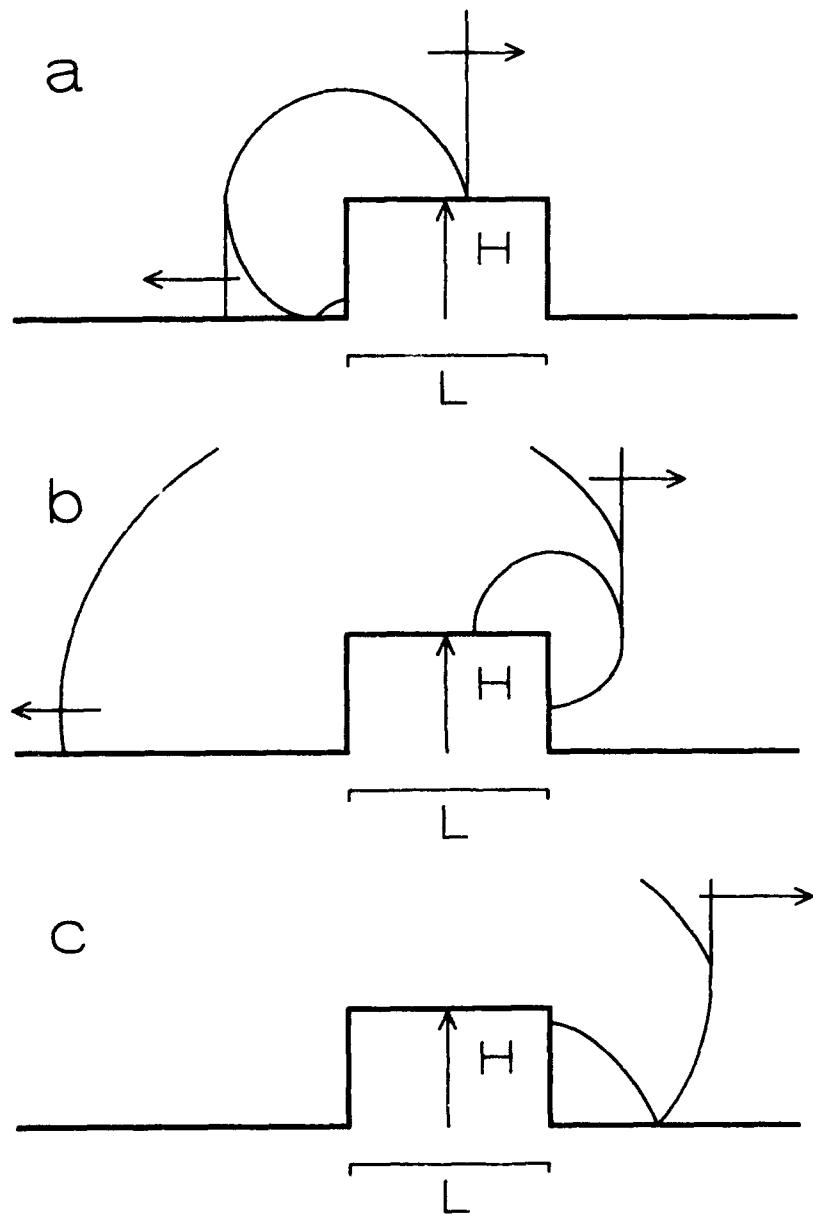
Figure 1   The reflection of a plane shock from a rectangular structure. In (a) the reflection on the front face is shown. In (b) the diffraction around the back edge is drawn and (c) shows the reflection of the diffracted wave from the ground (920536)

2.3   A set of Pi terms for diffraction loading

In this section a set of Pi terms is proposed for the description of the blast loading during the diffraction phase. The Pi terms relate to the development of the blast density with time and are combined by the formulation of a new scaling law. The derivation is based on the observations made for blast

loading on a rectangular structure ([2], see also section 2.2). For simplicity it is assumed that the positive phase of the blast is very long, i.e. during the diffraction over the structure the blast wave behaves like a plane uniform shock. Then the important physical parameters are

- the density ρ_0 [kg/m^3] and the velocity of sound c_0 [m/s] in ambient air,
- the shock velocity U_s [m/s],
- the length l [m] and the shape parameters α_i of the structure,
- and the time t [s].

According to Equation (4) the overpressure p_s and the shock velocity U_s are mutually dependent; U_s is chosen as a parameter instead of p_s, because in the discussion of section 2.2 the dimensionless term (U_s t / l) plays an important role.

The density ρ_0 was chosen as a parameter instead of the ambient pressure p_0, since the measurements yield as output the density distribution $\rho(x,y)$ around a structure. It can be expressed in dimensionless terms as

$$\rho(x,y)/\rho_0 = \Omega(M_s, U_s t/l, x/l, y/l, a_i) \tag{7}$$

$M_s = U_s/c_0$ is the Mach number of the shock and Ω is a complicated function of its arguments. A better scaling law for blast loading than Equation (7) is suggested by Equation (5). For shocks of moderate strength p_s the dynamic pressure q is small and Equation (5) can be written as

$$p_r/p_s = 2 \tag{8}$$

i.e. the quantity p_r/p_s is independent of p_s. Equation (8) is the reflection factor in the linear-acoustic limit, but it can also be used as an approximate scaling law for nonlinear reflection processes. A relation similar to (8) holds for the density in a reflected wave, so it is suggested to replace Equation (7) by

$$(\rho(x,y)-\rho_0) / (\rho_s-\rho_0) = \Omega'(U_s t/l, x/l, y/l, a_i) \tag{9}$$

where ρ_s is the density in the shock. It depends on M_s [2,3]:

$$\rho_s/\rho_0 = 6 M_s^2 / (M_s^2 + 5) \tag{10}$$

The term ρ_s-ρ_0 in Equation (9) is the density jump in the shock and thus it is the density analogue of the overpressure p_s. The importance of Equation (9) is that the function Ω' depends on the position $x_s = U_s t$ of the shock and not on M_s (or equivalently, the shock strength).

The scaling law (9) is developed for blast loading at moderate overpressures ($p_s < 100$ kPa). In a given situation the validity of the scaling law depends essentially on two factors:

- the deviation of the reflection factor from the linear acoustic value, and

- the importance of the air flow in the blast for the propagation of expansion waves.

In addition, the possible appearance of vortices at the edges of the structure can cause errors in the blast loading obtained from a scaling procedure.

An impression of the approximate nature of the scaling law in the target range of pressures is obtained by considering the process of normal shock reflection by an infinite wall, where calculations with Equation (9) yield $\Omega' = 2.006$, 2.055 and 2.440 for points (x,y) in the reflected shock, at Mach numbers M_s of respectively 1.004, 1.041 and 1.359 ($p_s = 1$, 10 and 100 kPa). Thus the loading by reflected waves is scaled with an error of at most 22 %. In the next Chapters an experiment is discussed, which investigates the accuracy of the new scaling law for a complicated diffraction process, with an emphasis on the description of expansion waves.

3   THE EXPERIMENTAL CONFIGURATION

This section describes the structure, which was chosen to validate the scaling law (9), and the configuration of the detectors in the experiments. In addition the motivations for chosing this particular setup are discussed.

The measurements were performed with the 40x40 cm^2 shock tube of the TNO Prins Maurits Laboratory. Piezoresistive pressure transducers can be attached to the tube at regular intervals of 0.5 m and the flow field at the measuring site can be visualized with a shearing interferometer. A description of the shock tube specifications and the operation of the interferometer can be found in reference [4]. Quantitative information about the density distribution of the flow field is obtained from the interferograms by means of the fringe counting technique.

The model of a shelter was placed at the measuring site. The side of the shelter facing the incident shock is a wedge with an angle of 35°. The length of the wedge is 5.0 cm, i.e. half the length of the shelter. The other half of the shelter is rectangular (model dimensions: 5.0x3.5 cm^2) with a flat roof at the same height as the top of the wedge. The advantage of constructing the shelter in the shape of a wedge is that the shock is reflected upwards and not upstream, as for the rectangular structure in section 2.2. Therefore the overpressure of the reflected shock on the front face of the shelter can decay immediately by an upstream-moving expansion wave.

In the experiments plane shocks with peak pressures of 6.5 kPa and 33.2 kPa were used. The positive phase of the blast waves is approximately 20 ms, so during the diffraction process they behave as uniform shocks. The choice of their strengths was motivated by two arguments:

1 the values are the boundaries of a range of pressures, where the shearing interferometer operates with sufficient resolution for a quantitative analysis of the interferograms;

2 shock wave theory predicts regular reflection at the wedge for a peak pressure of 6.5 kPa, whereas Mach reflection occurs at 33.2 kPa [5, 6]. It is interesting to investigate if scaling laws are valid in spite of the differences in the reflection process.

Interferograms of the blast loading on the shelter were recorded in time steps of 40 µs, starting from the point of time where the shock front reaches the foot of the wedge. An objective of the measurements was to determine the density of air around the shelter, which is impossible if large density gradients (e.g. shocks) are present in the shearing direction. Therefore, the interferometer was used with x-shear and the fringe counting analysis started from the left, in the tail of the blast wave. The procedure followed in the ordering of the fringes is described in Annex 1.

4   RESULTS

4.1   The experimental data

Figure 2 shows the overpressure as a function of time for blast waves, which were generated with driver fillings of compressed air at overpressures of 0.5 bar (a) and 4 bar (b). The pressure transducer was mounted at a distance of 14.6 cm from the foot of the wedge. About 1 ms after the arrival of the shock front an increase in pressure is observed due to the reflection of the shock from the wedge. For each driver filling the experimental programme consisted of a series of 13 shots; the average strength of the shocks is respectively (6.48 ± 0.15) kPa and (33.2 ± 0.7) kPa.

Interferograms of the blast loading were recorded on Kodak TXP 6049 film in steps of 40 µs, starting from the point where the shock front reaches the foot of the wedge. Figure 3 shows interferograms for the peak pressure of 6.5 kPa, at times t=80 µs (a), 200 µs (b), 320 µs (c) and 480 µs (d). The interferograms in Figure 4a-d are recorded at the same time points, but in this case the peak pressure is 33.2 kPa. The shock front S, the reflection R from the wedge and the expansion waves E_1 and E_2 at the two upper edges of the model are clearly visible. The negatives of the interferograms were digitized with a CCTV camera and analyzed with the computer code PCImage [7] on a µVAX-3300.

Max: 0.8136E+01 t= 1.612 [ms] Min: -0.1610E-01 t= 0.226 [ms]

Max: 0.3954E+02 t= 1.582 [ms] Min: -0.1115E+01 t= 0.466 [ms]
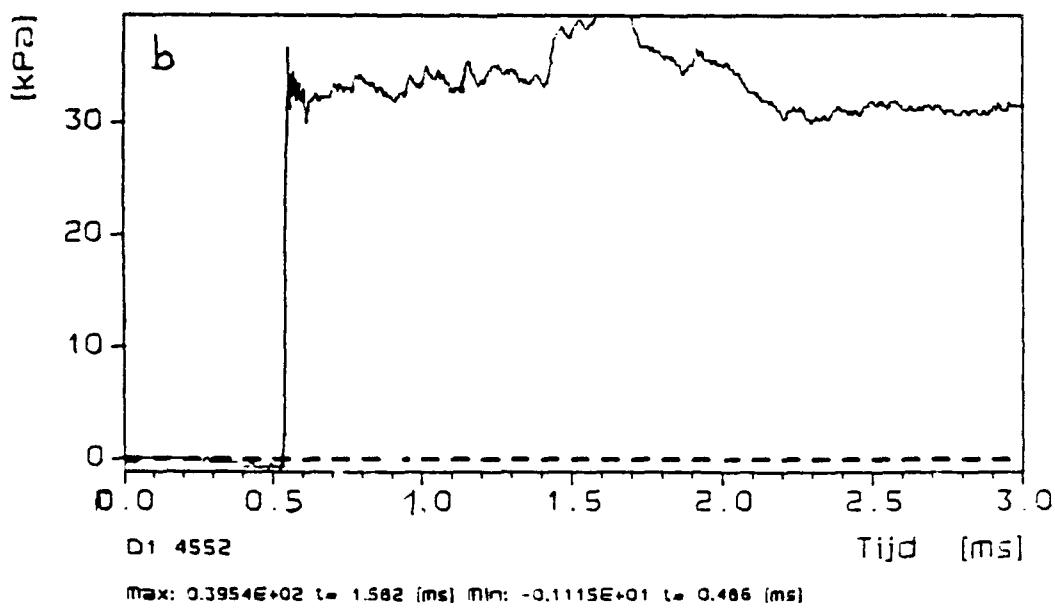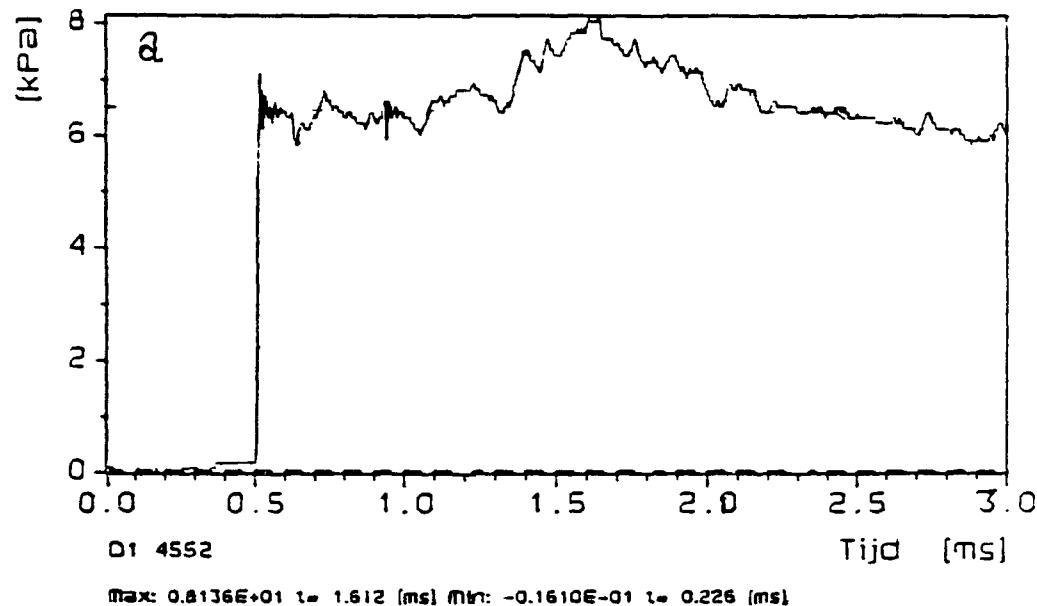
Figure 2   The variation of pressure with time measured at a distance of 14.6 cm in front of the
               model, for driver fillings of 0.5 bas (a) and 4 bar (b) (92537)
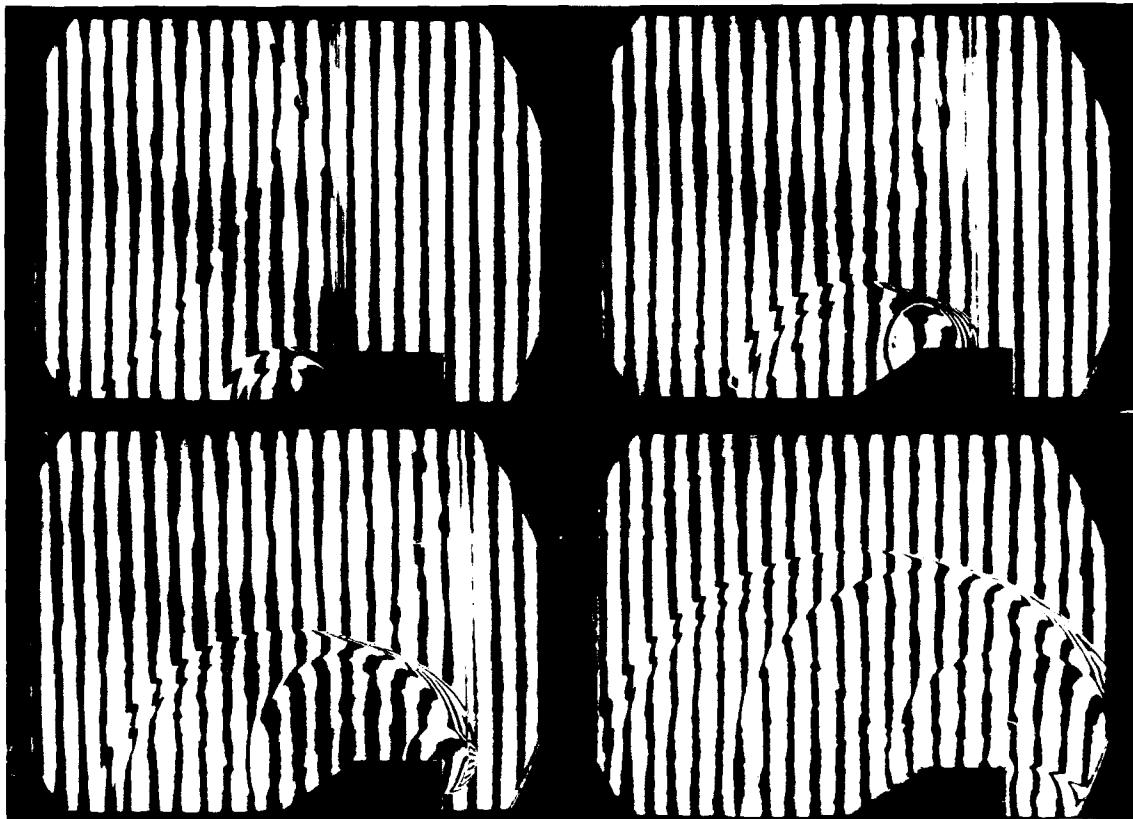
Figure 3   Interferograms of the blast loading on the model, recorded at times t=80 μs (a), 200
                μs (b), 320 μs (c) and 480 μs (d). The driver contained compressed air at an
                overpressure of 0.5 bar (910203-4, -7, -11, -16)
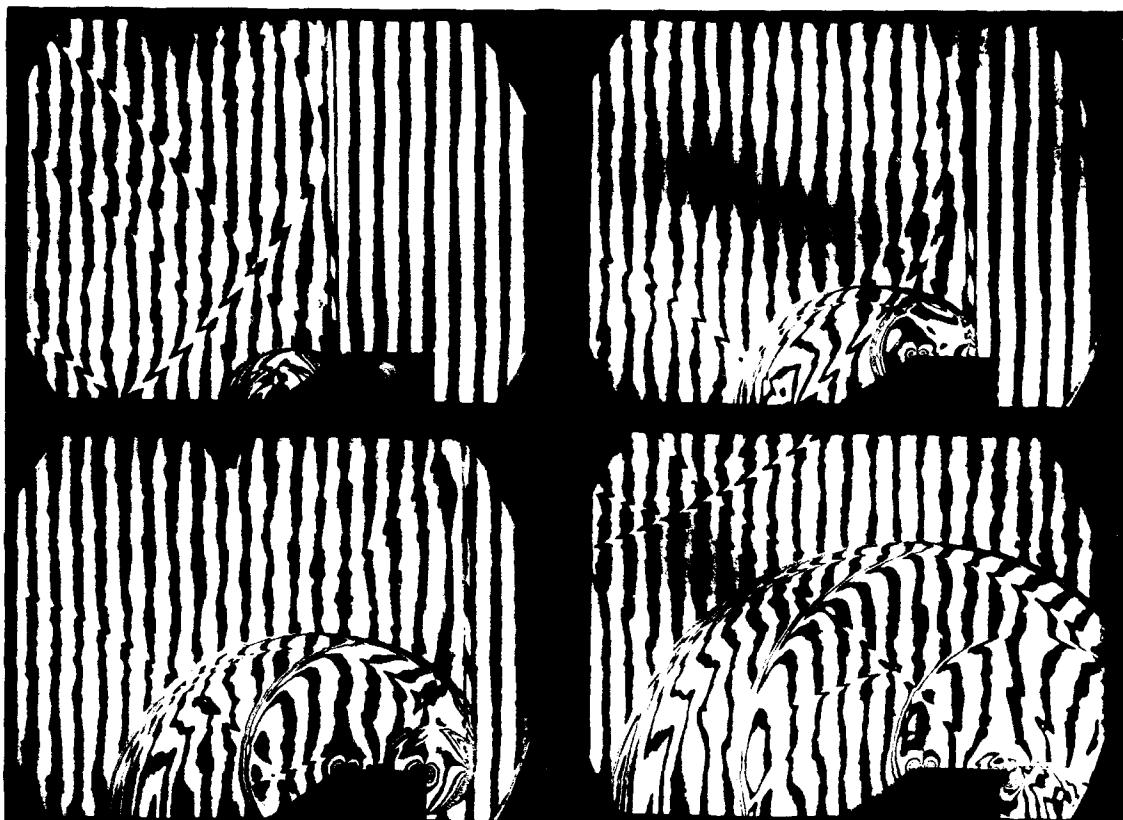
Figure 4   Interferograms of the blast loading on the model, recorded at times t=80 μs (a), 200 μs (b), 320 μs (c) and 480 μs (d). The driver contained compressed air at an overpressure of 0.5 bar (910204-4, -7, -11, -16)

4.2   The S-, R- and E-wave velocities

It is obvious from the Figures 3 and 4, that the velocity of S-, R- and E-waves is different for the two peak pressures. In the analysis of two series of 13 interferograms a ratio of (1.129 ± 0.017) was found for the S-wave velocities U_S at 33.2 kPa and 6.5 kPa. The velocities of the R-wave and the E-waves were also determined for both series, under the assumption that their value remains constant between t = 0 and 480 μs. In Table 1 the results are expressed relative to the S-wave velocities U_S. The Table also contains the statistical error of the values. The value of u_R in vertical direction contains an additional systematical error due to uncertainties in matching the x- and y-scale, which is not included in the error value.

Table 1   The velocities of R- and E-waves relative to the velocity of the shock. The values are
               derived from the interferograms at 6.5 kPa and 33.2 kPa under the assumption that
               the wave velocity is a constant

velocity	direction	value (in U_s) for p=6.5 kPa	value (in U_s) for p=33.2 kPa
$u_R(y=0)$	-x	0.971 ± 0.017	0.760 ± 0.011
$u_R(x=\text{foot of wedge})$	y	1.047 ± 0.013	0.974 ± 0.015
$u_{E1}(y=H)$	-x	0.91 ± 0.04	0.82 ± 0.06
$u_{E2}(y=H)$	-x	0.89 ± 0.04	0.72 ± 0.06

4.3   The density distribution

The fringe counting technique was applied in order to determine the density at three locations on
the wedge: y=0.08 H, 0,40 H and 0.73 H (H=0.35 l is the height of the model). On the top face the
location was selected in the middle, since the density distribution near the edges is affected by the
vortices. In a vortex a strong density drop occurs, which leads to an accumulation of fringes; in
addition, errors are introduced due to the refraction of the light rays. In order to avoid the vortices
during the counting of fringes, the density on the top face was actually determined somewhat
higher, at y=1.2 H.

Due to the uncertainty in the fringe positions only density gradients with values between 0.2 and
7 kg/m^4 could be resolved, but this was sufficient to analyze most of the interferograms. An
example of the analysis of a complicated interference pattern is given in Annex 2. Annex 2 also
contains examples of the variation of the density distribution with time.

The results of the analysis were expressed in the Pi terms of Equation (9). Figure 5 shows the
scaled density on the wedge at a height y=0.08 H as a function of the scaled time, for p_s = 6.5 kPa
(open dots) and 33.2 kPa (full dots). The vertical dashed line is the time of arrival of the shock. The
horizontal dashed line is the calculated strength of the reflected shock at 6.5 kPa, which was
obtained from Equation (9) under the assumption of regular reflection [5]. The strength could not
be calculated at 33.2 kPa, since in this case Mach reflection occurs at the wedge. The arrows indicate
the scaled times of arrival of the expansion wave E_1 for the two shock strengths. Similarly, in
Figures 6 and 7 the scaled density on the wedge is shown as a function of the scaled time, at heights
of respectively y=0.40 H and y=0.73 H. Figure 8 shows the scaled density in the middle of the top
face of the model. The arrows indicate the scaled times of arrival of the expansion wave E_a for the
two shock strengths.

○   6.5 kPa   ●   33.2 kPa

2.5

exp

2.0

exp

Scaled density [–]   1.5

1.0

0.5

0.0

0.0   0.5   1.0   1.5   2.0   2.5
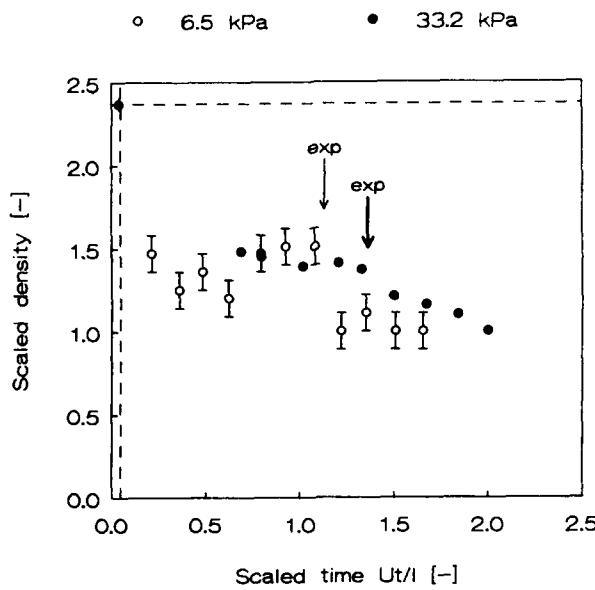
Scaled time Ut/l [–]

Figure 5   The scaled density as a function of the scaled time, determined on the wedge face at a
height y=0.08 H. Open and full dots indicate the results at shock strengths of
respectively 6.5 kPa and 33.2 kPa. The vertical and horizontal dashed lines are
respectively the time of arrival of the shock and the density calculated for regular
reflection. The arrows indicate the arrival of E_1 (920538)

○   6.5 kPa   ●   33.2 kPa

2.5

2.0   exp
exp

Scaled density [–]   1.5

1.0

0.5

0.0

0.0   0.5   1.0   1.5   2.0   2.5
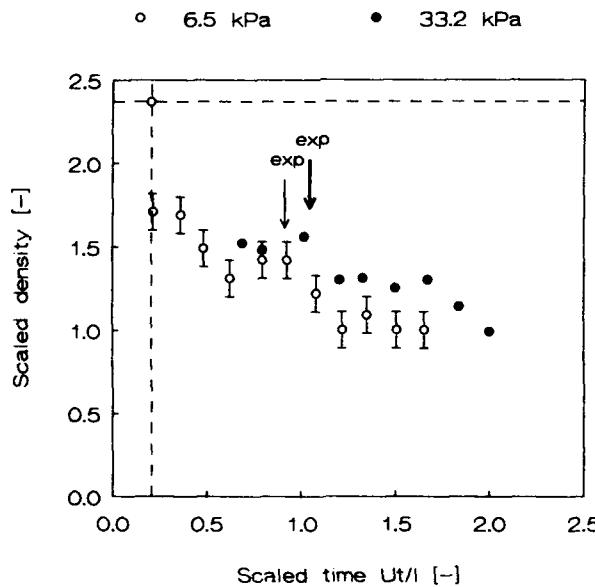
Scaled time Ut/l [–]

Figure 6   The scaled density as a function of the scaled time, determined on the wedge face at a
height y=0.40 H. Open and full dots indicate the results at shock strengths of
respectively 6.5 kPa and 33.2 kPa. The vertical and horizontal dashed lines are
respectively the time of arrival of the shock and the density calculated for regular
reflection. The arrows indicate the arrival of E_1 (920539)
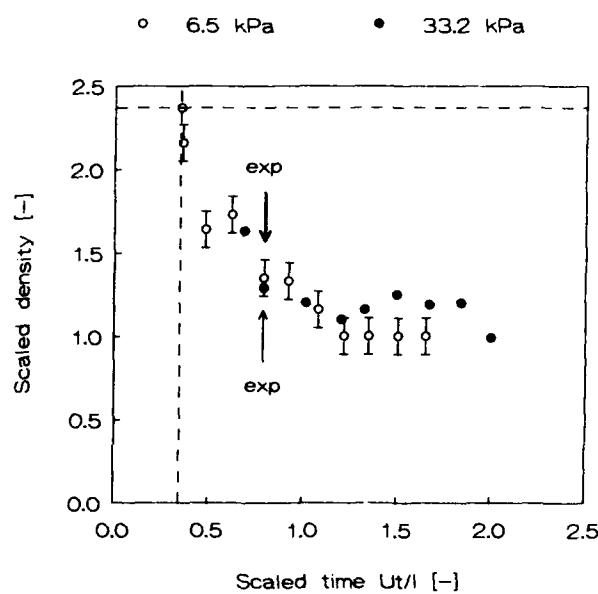
Figure 7   The scaled density as a function of the scaled time, determined on the wedge face at a height y=0.73 H. Open and full dots indicate the results at shock strengths of respectively 6.5 kPa and 33.2 kPa. The vertical and horizontal dashed lines are respectively the time of arrival of the shock and the density calculated for regular reflection. The arrows indicate the arrival of E_1 (920540)
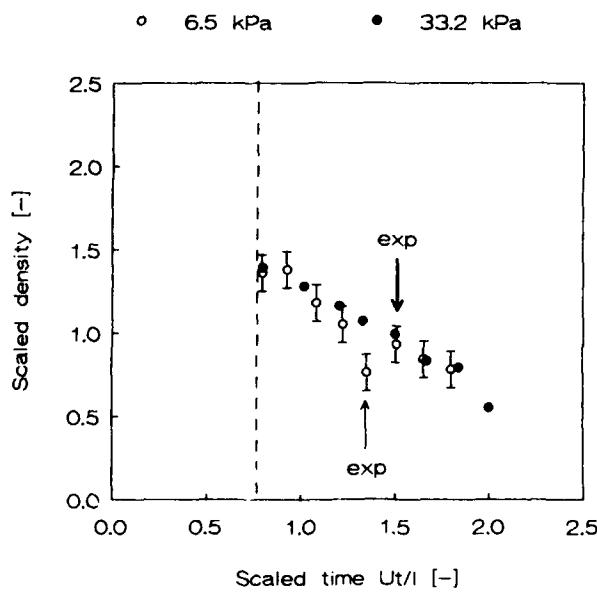


Figure 8   The scaled density as a function of the scaled time, determined on the middle of the top face at a height y≈1.2 H. Open and full dots indicate the results at shock strengths of respectively 6.5 kPa and 33.2 kPa. The vertical dashed line is the time of arrival of the shock. The arrows indicate the arrival of E_2 (920541)

5 DISCUSSION

5.1 The S-, R- and E-wave velocities

The main purpose for determining the wave velocities was to investigate the importance of the shock strength for the process of diffraction loading. Wave propagation depends strongly on the density distribution of the flow field. Therefore differences, which are observed between the data sets at 6.5 kPa and 33.2 kPa, give information about the validity of the scaling law (9).

According to Equation (4) the Mach numbers $M_s = U_s/c_0$ corresponding to the overpressures of (6.48 ± 0.15) kPa and (33.2 ± 0.7) kPa are respectively (1.0270 ± 0.0006) and (1.132 ± 0.003). Their ratio, (1.102 ± 0.003), is somewhat less than the value of (1.129 ± 0.017), which was derived from the interferograms. Apparently velocity calculations from the shock overpressure with Equation (4) contain a small systematic error.

The results in Table 1 show that the R-wave moves upward with approximately the velocity of the incident S-wave. In horizontal direction the R-wave and the E-waves propagate slower than the S-wave. The main reason for this difference is the flow of air behind the shock front, which decelerates upstream-moving waves. An upstream-moving sound wave has a velocity

$$u_c = c_1 - u_1 \tag{11}$$

where c_1 is the local velocity of sound and u_1 is the velocity of the air flow. Expressions for c_1 and u_1 can be derived from the shock adiabatic [2]. They are [2,3]

$$c_1/c_0 = \sqrt{(1 + p_s/p_0)(7 + p_s/p_0)/(7 + 6p_s/p_0)} \tag{12}$$

and

$$u_1/c_0 = 5(p_s/p_0)/(7 M_s) \tag{13}$$

Insertion of the appropriate values for p_s, p_0 and M_s gives values of 0.937 and 0.738 for u_c/U_s at respectively 6.5 kPa and 33.2 kPa (error values are omitted since the systematical errors are unknown). The calculated values of u_c agree with the values in Table 1, which indicates that the R- and E-waves propagate as sound waves.

It is clear from Table 1 that the R- and E-waves at $p_s=33.2$ kPa propagate upstream with a smaller velocity than at 6.5 kPa. The larger shock strength is accompanied by a faster air flow behind the wave front and, according to Equation (11), this reduces u_c.

5.2 The density distribution

In section 5.1 it is found that the wave propagation depends on the shock strength. This suggests that scaling laws, which base the time behaviour on the Pi term (U_s t / l), are of limited validity. In Figures 5 and 6 discrepancies up to 30 % are indeed observed between the data at 6.5 kPa and 33.2 kPa; however, in view of the large difference in shock strength the result of the scaling law is quite satisfactory. This is especially so, since the theory predicts different reflection processes at the wedge, e.g. regular reflection at 6.5 kPa and Mach reflection at 33.2 kPa [5]. Apparently there is no drastic change in the loading by the transition from regular reflection to Mach reflection.

The experimental values of the scaled density at the wedge are much lower than the theoretical value, which is calculated for an infinite plane ([5]; see also the point on the vertical dashed line in the Figures). The reason is that the circular part of the R-waves in the Figures 3a and 4a is an expansion wave, which attenuates the reflected wave [8]. Since the process of reflection from a wedge is an important topic in the theory of blast loading, a detailed description is given in Annex 3. It is concluded that the loading on the wedge face consists of a sharp peak due to the the unattenuated, reflected shock followed by a period of moderate loading by the circular R-wave. The expansion wave E_1 from the leftmost top edge of the model reduces the density on the wedge face to the density ρ_s in the incident blast wave. From the Figures 5, 6 and 7 it can be seen that this situation is reached at a time t = $2l/U_s$.

According to Figure 8 the density on the top face is initially somewhat larger than ρ_s. The arrows indicate the times of arrival of the expansion wave E_2 from the rightmost top edge of the model. This wave reduces the density to a value below ρ_s. The Figures 3d and 4d show that the E_2-wave reflects from the bottom behind the model. The measurements were ended at this point, because the fringe counting technique could no longer be applied. It is expected that the reflection on the bottom will expand over the rightmost edge and raise the density on the top face to ρ_s. From that time the loading will be mainly caused by the drag force.

In the present work the loading on the model is expressed in terms of the density distribution on the wedge and the top face. This is a convenient choice for the presentation of the experimental results,

however, usually the interesting quantity is the pressure. The pressure is related to the density by the entropic equation of state

$$p(x,y,z) = 0.4 \, \rho(x,y,z)^{1.4} \, e^{[S(x,y,z)-S_0]/C_v} \tag{14}$$

where $S(x,y,z)$ is the entropy, S_0 is a constant and C_v is the specific heat at constant volume. The shocks used in the present work were of moderate strength and then $S(x,y,z)$ is approximately constant in the whole flow field. For such cases the exponent in Equation (14) is a constant and the pressure distribution can be calculated directly from the density with the Equation

$$p[\text{in kPa}] = 78.04 \, (\rho[\text{in kg/m}^3])^{1.4} \tag{15}$$

6   CONCLUSIONS AND RECOMMENDATIONS

The loading of blast waves on a model of a shelter was studied in the 40x40 cm^2 blast simulator of the TNO Prins Maurits Laboratory. The velocities of wave propagation and the density in the flow field were determined at several locations by means of flow visualization with a shearing interferometer. A new scaling law, which eliminates the strength of the blast wave from the description of the loading on the model, was developed for peak overpressures p_s below 100 kPa. The scaling law expresses the time behaviour of the loading as a function Ω, whose arguments are dimensionless Pi terms:

$$(\rho(x,y)-\rho_0) / (\rho_s-\rho_0) = \Omega(U_s t/l,\ x/l,\ y/l,\ a_i) \tag{9}$$

In (9) U_s is the shock velocity, t is the time, l is the length and a_i are shape parameters of the model, (x,y) are space coordinates and $\rho(x,y)$, ρ_s and ρ_0 are respectively the density distribution, the density in the shock and the density of ambient air. Equation (9) is formulated in terms of the density, which was the measured quantity in the experiments, but a similar relation exists for the pressure. It was found that the propagation of the secondary waves originating from reflection and expansion was different for shock strengths of 6.5 kPa and 33.2 kPa, mainly due to the air flow in the incident shock. In spite of this fact, the scaling law (9) gave similar blast loadings on the front and top face of the model for both shock strengths.

The present work proves that the scaling law (9) can be applied for shocks of moderate strengths in the diffraction phase. The important point is that the blast loading is essentially determined by the shape parameters of a given structure, so it is sufficient to perform measurements at one shock strength. Then Equation (9) gives an approximation of the blast loading at other shock strengths, which in many cases will be of an acceptable accuracy (differences of at most 30 % were observed between the loading on a structure at 6.5 kPa and 33.2 kPa).

The scaling law (9) is useful in many research areas of blast loading. It can be used as input for a finite-element code, when the possible failure of a structure for various peak overpressures is investigated. Another application is the estimation of blast loading on a structure at destructive peak overpressures by performing measurements at much lower pressures. Finally, the scaling law implies that a structure can be designed in a blast-resistant shape for a large range of pressures, which makes it worth while to develop criteria for such a design.

7   AUTHENTICATION

The author would like to thank Michel Dirkse for performing the measurements and Theo Verhagen for supplying the computer code PCImage.

E.A. Bakkum
(Project Manager/Author)

8   REFERENCES

1 Baker W.E., Westine P.S. and Dodge F.T, Similarity Methods in Engineering Dynamics, Hayden Book Company (New Jersey, 1973)

2 Landau L.D. and Lifshitz E.M., Fluid Mechanics, Pergamon Press (London, 1987)

3 Glasstone S. and Dolan P.J., The Effects of Nuclear Weapons, US Dept. of Defense and US Dept. of Energy (1977)

4 Bakkum E.A. Flow visualization with a shearing interferometer, Report No. PML1990-IN25 (Rijswijk, 1990)

5 Courant R. and Friedrichs K.O., Supersonic Flow and Shock Waves, Interscience Publishers (New York, 1948)

6 Kingery C.N. and Coulter G.A., Reflected overpressure impulse on a finite structure, Techn. Report ARBRL-TR-02537 (Aberdeen Proving Ground, 1983)

7 Verhagen Th.L.A., private communication (Rijswijk, 1990)

8 Heilig W., The Pseudo-Steady Shock Reflection Process as Predicted by the von Neumann Theory and by the SHARC-Code, in Festschrift zum 65. Geburtstag von Dr. Rer. Nat. H. Reichenbach (Freiburg, 1990)

9   SYMBOLS AND INDICES

9.1   Latin symbols

C   drag coefficient   -

c_0 velocity of sound in ambient air   m/s

c_1 velocity of sound in the shock   m/s

F   frictional force   N

l   length of the model   m

M_s Mach number of the shock   -

p_0 pressure of ambient air   Pa

p_r pressure of the reflected shock   Pa

p_s peak pressure of the shock   Pa

q   dynamic pressure   Pa

r   distance from the explosion centre   m

R_e Reynolds number   -

S   entropy   J/kg K

t   time   s

u_0 velocity of steady air flow   m/s

U_s velocity of the shock   m/s

u_1 velocity of air flow in the shock   m/s

W   charge size   N m

x,y,z   space coordinates   -

9.2   Greek symbols

η viscosity of ambient air   poise

Ω function   -

ρ_0 density of ambient air kg/m^3

ρ_s density in the shock kg/m^3

ANNEX 1   DETERMINATION OF THE ORDER IN THE FRINGE COUNTING
            TECHNIQUE

In shearing interferometry the density gradient of the flow field can be calculated from phase shifts in a light beam. Unfortunately the interferograms only record the maxima and minima in the interference pattern (corresponding to phase differences of respectively $2\pi N$ and $2\pi(N+\frac{1}{2})$), but they contain no information about the phase distribution between extrema. A careful procedure is required for determining the fringe order N. In this Annex the rules, which were applied in the process of fringe counting, are summarized. They are:

- the interferograms were recorded in finite-fringe mode [4]; the Wollaston prism of the interfero-
  meter was positioned in such a way that the order of the reference fringes decreases from left to
  right;

- fringe counting starts from the left, in the region where the blast wave is still unperturbed;

- the analysis is restricted to fringes corresponding to a maximum;

- if fringes are separated by a minimum, they usually differ ± 1 in order; in some exceptional cases
  they are of the same order;

- in most cases the order can be derived from the reference fringes, however, for closed fringes this
  is not possible. Then use is made of basic knowledge about fluid flow: the density increases by
  the reflection of a pressure wave and decreases in an expansion wave; the density decreases
  towards the centre of a vortex;

- sometimes the order of closed fringes can be deduced from the systematic behaviour of other
  fringes with known order in the interferogram;

- sometimes the order of closed fringes in an interferogram can be derived by a comparison with
  the fringe patterns in preceding and successive interferograms.

ANNEX 2   EXAMPLES OF THE ANALYSIS OF AN INTERFERENCE PATTERN

This Annex gives examples of density distributions, which were deduced from the two series of 13 interferograms (see Chapter 3). The analysis is based on the fringe counting technique, which is summarized in Annex 1. The intermediate steps in the analysis are illustrated in the first part of this Annex. The second part shows the development of the density distribution in the reflected wave as a function of time.

2.1A   The analysis

Figure 1aA shows the ordering of fringes, which was obtained at a height y = 1.2 H in Figure 4c of the main text, by application of the procedure in Annex 1. In finite-fringe mode a tilt is introduced in the fringe distribution by placing the Wollaston prism of the shearing interferometer outside the focus of the mirror system. This artificial tilt is represented in Figure 1aA by a dashed line. The density gradient corresponding to the fringe distribution is drawn in Figure 1bA [4,7]. The gradient is positive in the reflected wave and negative in the expansion waves. Figure 1bA also shows the behaviour of the gradient in a density dip: at the leftmost vortex the gradient is at first negative but becomes positive after passage of the centre. The peak on the right side is artificial and indicates the position of the shock front. Figure 1cA shows the density distribution, which is calculated by an integration of the gradient in Figure 1bA over the horizontal coordinate. The integration constant is the value of the density at the lower boundary of integration, i.e. in the unperturbed blast wave. It was calculated with

$$\rho = \rho_0 \left[7 + 6 \, (p_s/p_0) \right] / \left[7 + (p_s/p_0) \right] \tag{1A}$$

where p_s is the overpressure and p_0 and ρ_0 are respectively the ambient pressure and density. Equation (1A) is derived from Equations (4) and (10) in the main text. Insertion of $p_s = 33.2$ kPa, $p_0 = 101.3$ kPa and $\rho_0 = 1.205$ kg/m^3 in Equation (1A) gives $\rho = 1.474$ kg/m^3 for the integration constant.
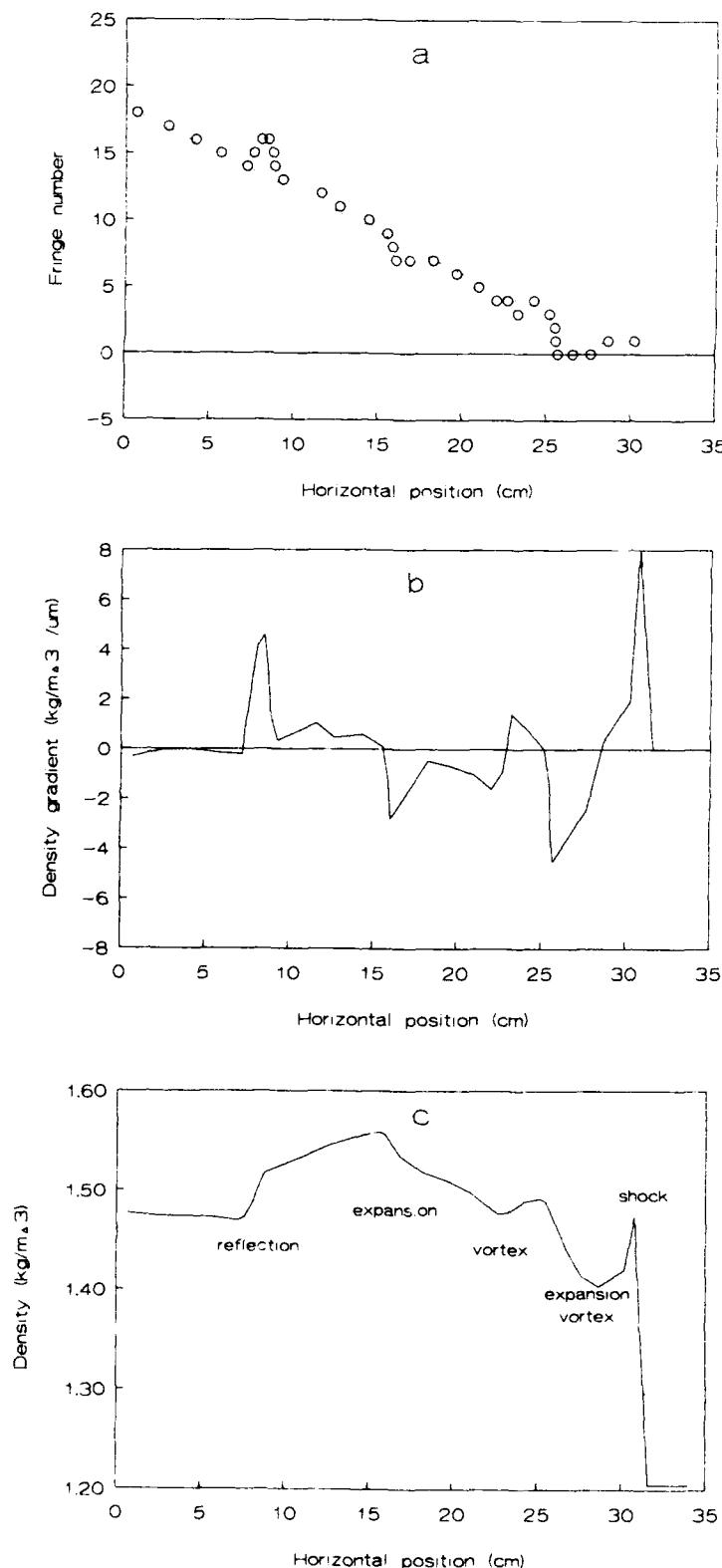
Figure 1A   The intermediate steps in the determination of the density distribution from Figure 4c of the main text, at a height y=1.2H. In (a) the fringe ordering is shown, (b) is the density gradient and (c) the density, obtained by integrating (b) (920542, 920543, 920544)

2.2A The density distribution in the reflected wave

The advantage of flow visualization over other techniques is that the behaviour of the complete flow field is recorded. From the recordings, the density distribution is obtained as a function of the spatial coordinates (x,y). If the flow field is recorded at successive time intervals, then the variation of density with time is also determined. This is illustrated in Figure 2A, which shows the variation of the density in the R-wave as a function of x, at a height y=0.73 H (arrow), for times t=120 μs (dot-dashed curve), 200 μs (solid curve), 280 μs (dashed curve) and 360 μs (dotted curve). The thick solid line indicates the position of the wedge. The curves in the Figures 2aA and 2bA were derived for shock strengths of respectively 6.5 kPa and 33.2 kPa. The Figures clearly show the propagation of the R-wave and its attenuation by the expansion wave E_1, which arrives at t=200 μs. At 33.2 kPa the R-wave exhibits a steep edge, which is not visible at 6.5 kPa.

In section 2.1A it was explained that shearing interferometry measures the density gradient and an integration is necessary in order to obtain the density. This procedure is successful for values of the density gradient between 0.2 and 7 kg/m^4. The R-wave in Figure 2aA is very weak and can just be resolved. In contrast, steep gradients are present in Figure 2bA and small errors in their value have a large impact on the calculated density. This explains the fact, that at a time t=280 μs on the average lower densities are calculated than at t=360 μs.
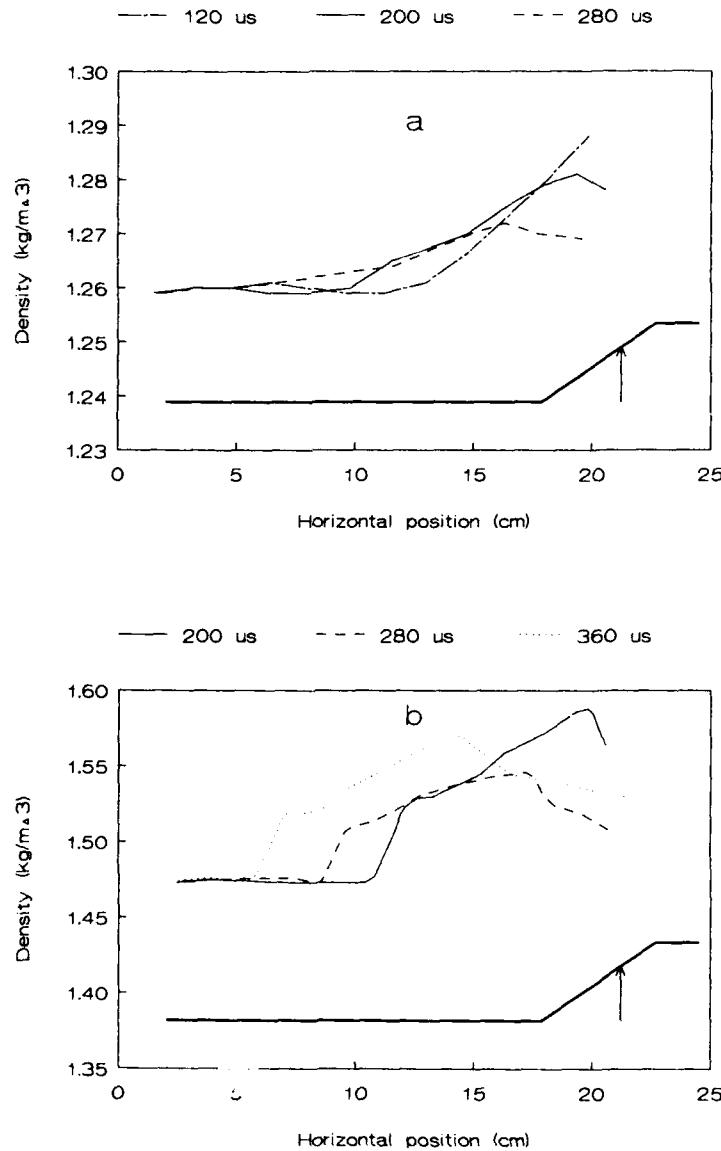
Figure 2A   The density distribution in the R-wave at a height y=0.73 H (arrow), at times t=120
              µs (dot-dashed curve), 200 µs (solid curve), 280 µs (dashed curve) and 360 µs
              (dotted curve). The thick solid line indicates the position of the wedge. In (a) and (b)
              the results for the shocks of respectively 6.5 kPa and 33.2 kPa are displayed
              (92545, 92546)

ANNEX 3   REGULAR REFLECTION FROM A WEDGE

The nonlinear behaviour of shock waves is of particular importance in reflection processes. It appears from experiments that the characteristics of the reflected wave depend on the strength of the incident wave (see reference [8] of the main text). In the case of oblique reflection of a plane, uniform shock wave from an infinite wall it is possible to derive analytical Equations for the strength and angle of the reflected shock. In the derivation use is made of the conservation of mass, momentum and energy across the shock front and the constraint that the air flow in the reflected shock is parallel to the wall (see reference [5] in the main text). The process that is described by these Equations is called regular reflection. Under certain conditions (skimming incidence of strong shocks) a solution of the Equations does not exist and a different process occurs, called Mach reflection [3,5,6,8].
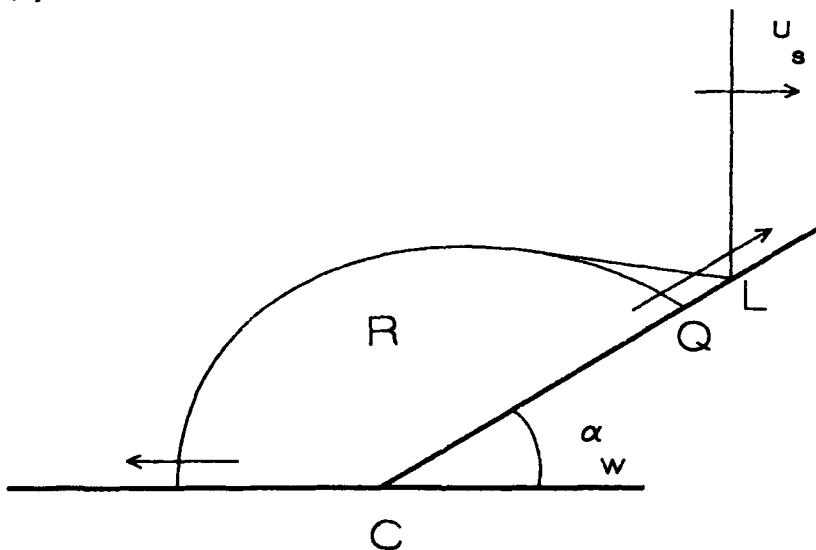

Figure 1B   Regular reflection of a uniform plane shock wave from a wedge (920547)

In practice the size of a wall is of course finite and boundary effects change the reflected wave. Figure 1B shows the process of regular reflection from a wedge. The reflected shock R is attenuated by a circular expansion wave, which emerges at the foot C of the wedge. Although the strength (i.e. overpressure or density) of the circular part of the R-wave is no longer uniform, the reflection process is still self-similar. This means that Figure 1B is valid for all times. A part of the expansion wave follows the reflected shock with the local velocity of sound. It has been suggested that Mach reflection occurs in situations where the expansion wave overtakes the shock front [8]. The part of the expansion wave, which travels upstream, is a weak shock wave.

Figure 1B is in fact a schematic drawing of the reflection process in the experiments at 6.5 kPa of the main text, at least until the shock front reaches the top of the wedge (see Figure 3a of the main text). Therefore calculations of regular reflection were performed for Figure 1B, assuming a wedge angle α_w of 35° and a peak overpressure of 6.5 kPa in the incident shock (ρ_s=1.260 kg/m^3 according to Equation (1A) of Annex 2). The intersection L of the wave front with the wedge face moves with a velocity

$$u_L = U_s/\cos(\alpha_w) = 1.254\, c_o \qquad (1B)$$

(see Equation (4) in the main text). The intersection Q of the circular wave with the wedge face moves with a velocity

$$u_Q = v_R + c_R \qquad (2B)$$

where v_R is the air flow velocity in the reflected shock and c_R is the local velocity of sound. Equation (2B) is comparable to Equation (11) of the main text, because they both describe the influence of air flow on wave propagation. Actually, in the discussion of the E_1- and E_2-wave velocities in the main text the use of Equation (2B) instead of (11) would have been more correct, because the expansion waves propagate in the reflected R-wave; Equation (11) was only chosen for the sake of simplicity. The quantities vR and cR can be calculated provided that the values of the density ρR and the peak overpressure pR in the reflected shock are known. Equations in the literature (92.9 and 92.10 in reference [2]; see also [5]) yield ρ_R=1.336 kg/m^3 and p_R=15.67 kPa. Then the constraint of mass conservation at the front of the reflected wave requires v_R=0.089 c_o and the equation of state yields c_R=1.021 c_o. Finally, application of Equation (2B) gives
$u_Q = 1.110\, c_o$.
Consequently the ratio u_L/u_Q is 1.130, and, because of self-similarity the ratio between the distances LC and QC in Figure 1B is also 1.130. Only a fraction (12%) of the wedge face is loaded with the unattenuated, reflected shock. Thus in the present experiments the duration of the loading was less than 16 μs. Therefore the unattenuated, reflected shock strength is not observed in the results of the Figures 5, 6 and 7 in the main text.
The calculations in the preceding paragraph are based on the theory of regular reflection and so they can not be repeated for the experiment at 33.2 kPa, where Mach reflection occurs.

REPORT DOCUMENTATION PAGE
(MOD NL)

1. DEFENSE REPORT NUMBER (MOD-NL) TD91-2834	2. RECIPIENT'S ACCESSION NUMBER	3. PERFORMING ORGANIZATION REPORT NUMBER PML1991-54
4. PROJECT/TASK/WORKUNIT NO. 292688314	5. CONTRACT NUMBER	6. REPORT DATE June 1992
7. NUMBER OF PAGES 30 (3 Annexes)	8. NUMBER OF REFERENCES 8	9. TYPE OF REPORT AND DATES COVERED Final

10. TITLE AND SUBTITLE

Scaling laws for diffraction loading by air blast
(Schalingswetten voor diffractie bij schokbelastingen)

11. AUTHOR(S)

Dr. E.A. Bakkum

12. PERFORMING ORGANIZATION NAME(S) AND ADDRESS(ES)

TNO Prins Maurits Laboratory
P.O. Box 45, 2280AA Rijswijk, The Netherlands

13. SPONSORING AGENCY NAME(S) AND ADDRESS(ES)

Hoofddirecteur DO-TNO
P.O. Box 6006, 2600 JA Delft

14. SUPPLEMENTARY NOTES

15. ABSTRACT (MAXIMUM 200 WORDS (1044 BYTE))

The assessment of the damage, which is done to structures by an explosion, depends both on the blast loading and the structural response. In the past scaling laws were developed for the description of simple blast loadings, thus eliminating the need for full-scale experiments. The aim of this work is to construct an approximate scaling law for complex blast loadings.

The blast loading on a model of a shelter was studied in the 40×40 cm^2 blast simulator of the TNO Prins Maurits Laboratory. The density distribution around the model was determined by means of flow visualization with a shearing interferometer. An approximate scaling law, which eliminates the dependency on the shock strength, is proposed for the time behaviour of the blast loading. The scaling law is confirmed by measurements of the density at various locations on the model, for shock strengths of 6.5 kPa and 33.2 kPa.

16. DESCRIPTORS	IDENTIFIERS
Blast loading	Structural Response
Structures	Scaling
Air blast	Flow Visualization
Models	Density Measurement

17A. SECURITY CLASSIFICATION (OF REPORT) UNCLASSIFIED	17B. SECURITY CLASSIFICATION (OF PAGE) UNCLASSIFIED	17C. SECURITY CLASSIFICATION (OF ABSTRACT) UNCLASSIFIED
18. DISTRIBUTION AVAILABILITY STATEMENT Unlimited distribution		17D. SECURITY CLASSIFICATION (OF TITLES) UNCLASSIFIED

Distribution list

1	Hoofddirecteur DO-TNO
2	D.W.O.O
3	HWO-KL
4/5	HWO-KLu
6/7/8	TDCK
9	Lid Instituuts Advies Raad PML Prof. drs. P.J. van den Berg
10	Lid Instituuts Advies Raad PML Prof. ir. M.A.W. Scheffelaar
11	Lid Instituuts Advies Raad PML Prof. ir. H. Wittenberg
12	E.A. Bakkum, TNO-IMET Apeldoorn
13	PML-TNO, Programma directeur; daarna reserve
14/15	PML-TNO, sectie F
16	PML-TNO, archief
17	PML-TNO, documentatie